J. Fluid Mech. (2016), *vol.* 791, R3, doi:10.1017/jfm.2016.56

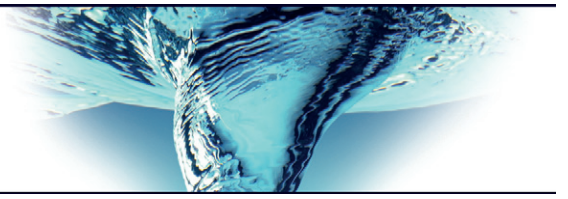

JFM RAPIDS
journals.cambridge.org/rapids

Azimuthal diffusion of the large-scale-circulation plane, and absence of significant non-Boussinesq effects, in turbulent convection near the ultimate-state transition

Xiaozhou He[1,2,6], **Eberhard Bodenschatz**[1,3,4,6] **and Guenter Ahlers**[1,5,6,†]

[1]Max Planck Institute for Dynamics and Self Organization (MPIDS), D-37073 Göttingen, Germany

[2]Institute for Turbulence–Noise–Vibration Interaction and Control, Shenzhen Graduate School, Harbin Institute of Technology, Shenzhen, China

[3]Institute for Nonlinear Dynamics, University of Göttingen, D-37073 Göttingen, Germany

[4]Laboratory of Atomic and Solid-State Physics and Sibley School of Mechanical and Aerospace Engineering, Cornell University, Ithaca, NY 14853, USA

[5]Department of Physics, University of California, Santa Barbara, CA 93106, USA

[6]International Collaboration for Turbulence Research

(Received 20 December 2015; revised 13 January 2016; accepted 18 January 2016; first published online 17 February 2016)

We present measurements of the orientation θ_0 and temperature amplitude δ of the large-scale circulation in a cylindrical sample of turbulent Rayleigh–Bénard convection (RBC) with aspect ratio $\Gamma \equiv D/L = 1.00$ (D and L are the diameter and height respectively) and for the Prandtl number $Pr \simeq 0.8$. The results for θ_0 revealed a preferred orientation with up-flow in the west, consistent with a broken azimuthal invariance due to the Earth's Coriolis force (see Brown & Ahlers (*Phys. Fluids*, vol. 18, 2006, 125108)). They yielded the azimuthal diffusivity D_θ and a corresponding Reynolds number Re_θ for Rayleigh numbers over the range $2 \times 10^{12} \lesssim Ra \lesssim 1.5 \times 10^{14}$. In the classical state ($Ra \lesssim 2 \times 10^{13}$) the results were consistent with the measurements by Brown & Ahlers (*J. Fluid Mech.*, vol. 568, 2006, pp. 351–386) for $Ra \lesssim 10^{11}$ and $Pr = 4.38$, which gave $Re_\theta \propto Ra^{0.28}$, and with the Prandtl-number dependence $Re_\theta \propto Pr^{-1.2}$ as found previously also for the velocity-fluctuation Reynolds number Re_V (He *et al.*, *New J. Phys.*, vol. 17, 2015, 063028). At larger Ra the data for $Re_\theta(Ra)$ revealed a transition to a new state, known as the 'ultimate' state, which was first seen in the Nusselt number $Nu(Ra)$ and in $Re_V(Ra)$ at $Ra_1^* \simeq 2 \times 10^{13}$ and $Ra_2^* \simeq 8 \times 10^{13}$. In the ultimate state we found $Re_\theta \propto Ra^{0.40 \pm 0.03}$. Recently, Skrbek & Urban (*J. Fluid Mech.*, vol. 785, 2015, pp. 270–282) claimed that non-Oberbeck–Boussinesq effects

† Email address for correspondence: guenter@physics.ucsb.edu

on the Nusselt and Reynolds numbers of turbulent RBC may have been interpreted erroneously as a transition to a new state. We demonstrate that their reasoning is incorrect and that the transition observed in the Göttingen experiments and discussed in the present paper is indeed to a new state of RBC referred to as 'ultimate'.

Key words: Bénard convection, turbulent convection

1. Introduction

Turbulent convection in a fluid contained between two parallel horizontal plates and heated from below (Rayleigh–Bénard convection or RBC; for reviews see Kadanoff (2001), Ahlers (2009), Ahlers, Grossmann & Lohse (2009*c*), Lohse & Xia (2010) and Chillà & Schumacher (2012)) contains two thin laminar boundary layers (BLs), one below the top and the other above the bottom plate, when the Rayleigh number Ra is not too large. When the fluid properties (except for the density where its temperature dependence drives the flow) are temperature-independent (Oberbeck–Boussinesq (OB) conditions; Oberbeck (1879) and Boussinesq (1903)), then both BLs are of equal thickness and each sustains an equal temperature difference nearly equal to $\Delta T/2$, where $\Delta T \equiv T_b - T_t$. Here, T_b and T_t are the temperatures at the bottom and top plates respectively. The sample centre temperature then is $T_c = T_m$, where $T_m \equiv (T_b + T_t)/2$. The fluid not too close to the BLs, known as the 'bulk', is strongly turbulent but nearly isothermal in the time average (see, however, Ahlers *et al.* (2012*a*), Ahlers, Bodenschatz & He (2014) and Wei & Ahlers (2014)), with a vigorously fluctuating temperature (He *et al.* 2014). The BLs emit thermal plumes at irregular time intervals which rise or fall through the bulk and, by virtue of their buoyancy, drive and in turn are carried by a large-scale circulation (LSC). For cylindrical samples with height L approximately equal to the diameter D (aspect ratio $\Gamma \equiv D/L \simeq 1$), the LSC consists of a single convection roll with rising fluid near the wall at an azimuthal location θ_0 and falling fluid also near the wall but close to $\theta_0 + \pi$.

The state of the system depends on $Ra \equiv g\alpha\Delta TL^3/(\kappa\nu)$ and the Prandtl number $Pr \equiv \nu/\kappa$. Here, g, α, κ and ν denote the gravitational acceleration, the isobaric thermal expansion coefficient, the thermal diffusivity and the kinematic viscosity respectively. The system described in the previous paragraph is referred to as 'classical' RBC. When Ra reaches a certain value Ra^*, it is expected theoretically (Kraichnan 1962; Spiegel 1971; Grossmann & Lohse 2011) that the laminar BLs of the classical state will also become turbulent due to the shear applied by the LSC, as well as by fluctuations on somewhat smaller scales. Above Ra^* the system is said to be in the 'ultimate' state, as this state is expected to persist up to arbitrarily high Ra (Chavanne *et al.* 1997). A theoretical estimate gave $Ra^* = O(10^{14})$ for Pr near 1 (Grossmann & Lohse 2002). Several experimental papers reported transitions found from measurements of the heat transport, expressed as the Nusselt number $Nu = \lambda_{eff}/\lambda$, where λ is the thermal conductivity of the quiescent fluid and $\lambda_{eff} = QL/(A\Delta T)$. Here, Q is the heat flux and A is the cross-sectional area of the cell. The results of Chavanne *et al.* (1997, 2001) and Roche *et al.* (2010) (the 'Grenoble' data, obtained with fluid helium at a temperature of approximately 5 K and a pressure of approximately 2 bars) found transitions in the Ra range from 10^{11} to 10^{12}, which in our view (but not that of the authors) is too low to correspond to a BL shear instability, although the data clearly show a sharp and continuous transition which, we believe, is of unknown origin (see Ahlers *et al.* 2012*b*). Measurements of Nu and of the Reynolds number $Re_V = VL/\nu$ (V is the root-mean-square fluctuation velocity) made with compressed

sulphur hexafluoride (SF_6) at ambient temperatures and pressures up to 19 bars also found a transition (Ahlers *et al.* (2012*b*), He *et al.* (2012*a*,*b*) and He *et al.* (2015); the 'Göttingen' data), but at $Ra^* \simeq 10^{14}$ in agreement with the theoretical estimate of Grossmann & Lohse (2002).

Here, we present a study of the azimuthal diffusivity D_θ of the LSC (§ 3.1). The LSC is a stochastically driven system, with the driving due to the small-scale fluctuations (Brown & Ahlers 2007*a*, 2008). In view of the rotationally invariant geometry of the cylindrical sample, θ_0 ideally should diffuse azimuthally in the presence of the stochastic driving and have a uniform probability distribution $p(\theta_0) = 1/(2\pi)$. However, in real experiments $p(\theta_0)$ always is found to have a maximum even when extraordinary care is used in preparing the sample cell, indicating that the rotational symmetry is broken by some external force or remaining internal imperfection. Nearly a decade ago, it was shown that the symmetry breaking by the Earth's Coriolis force is sufficient to yield the $p(\theta_0)$ observed in an experiment (Brown & Ahlers 2006*a*). A simple Navier–Stokes-based model for the azimuthal potential due to the Coriolis force revealed that θ_0 should be very close to west. Solving a Fokker–Planck equation with this model potential and a noise intensity derived from the measured D_θ yielded a $p(\theta_0)$ that agreed quantitatively with experiment. For that case the Prandtl number was 4.38 and $\Gamma = 1.00$. Two samples were investigated, one with $L = 24.8$ and the other with $L \simeq 50$ cm. The Rayleigh number was in the range $3 \times 10^8 \lesssim Ra \lesssim 10^{11}$.

The present study is for a physically larger sample, with $L = D = 112$ cm, and with the smaller $Pr \simeq 0.8$. Rayleigh numbers ranged from 2×10^{12} to 1.5×10^{14} and thus were much larger than in the previous work. Again, we found that the preferred θ_0 was close to west, consistent with the Earth's Coriolis force. We also measured D_θ and determined the corresponding Reynolds number $Re_\theta = L\sqrt{D_\theta/\nu}$. Comparison with an extrapolation of the earlier data indicates consistency with $Re_\theta \propto Pr^{1.2}$, a Prandtl-number dependence found before for Re_V (He *et al.* 2015). Quite remarkably, the diffusivity measurements confirmed that the ultimate-state transition occurs over a range of Ra, from $Ra_1^* \simeq 2 \times 10^{13}$ to $Ra_2^* \simeq 8 \times 10^{13}$, as was found earlier from measurements of $Nu(Ra)$ and $Re_V(Ra)$.

We also present new measurements of Nu which are for the same sample as that used for the study of the azimuthal diffusion. They, as well as Re_V measurements reported before (He *et al.* 2015) for a different sample with $\Gamma = 1.00$, reveal the ultimate-state transition and all three physical properties yield consistent results for Ra_1^* and Re_2^*, as shown below in figure 4.

Recently, it was claimed by Skrbek & Urban (2015) that the temperature dependence of fluid properties (non-OB conditions) may be responsible for the transitions seen in the Grenoble and Göttingen data and that hypothetical corresponding data for an OB system may not show any transitions. In § 4 we show two reasons why this claim is flawed.

2. Apparatus and procedure

The apparatus has been described elsewhere (Ahlers, Funfschilling & Bodenschatz 2009*b*; Ahlers *et al.* 2012*b*, 2014). It consisted of a sample cell located inside a vessel known as the 'Uboot of Göttingen' which was pressurized with sulphur hexafluoride (SF_6) at an average temperature $T_m = 21.5\,^\circ$C and at pressures that ranged from 2.0 to 17.7 bar, resulting in the relatively narrow Prandtl-number range from 0.78 to 0.86 over the Ra range from 2×10^{12} to 1.5×10^{14} (see figure 1*b* of Ahlers *et al.* (2014)).

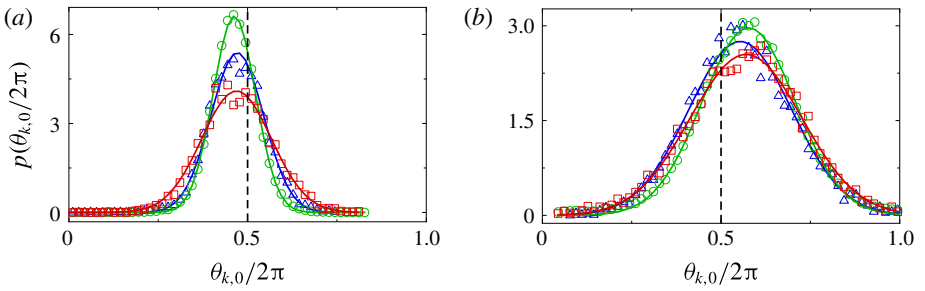

FIGURE 1. The probability distribution $p(\theta_{k,0}/2\pi)$ of the orientation $\theta_{k,0}/2\pi$ for (*a*) $Ra = 3.45 \times 10^{12}$ and (*b*) $Ra = 1.35 \times 10^{14}$, for $z/L = 0.25$ (red squares), 0.50 (green circles) and 0.75 (blue triangles). The solid lines represent fits of Gaussian functions to the data.

The Uboot had a volume of approximately 25 m^3, and approximately 2000 kg of SF_6 was required to fill it to the maximum pressure. The sample cell had aluminium plates at the top and bottom that were separated by a distance $L = 112$ cm and had an aspect ratio $\Gamma = 1.00$. The plates were levelled relative to gravity to $\pm 10^{-4}$ rad.

Three sets of eight thermistors, one each at the heights $z/L = 0.25$, 0.50 and 0.75, were embedded in the sidewall (Brown, Nikolaenko & Ahlers 2005). Since the LSC carries warm fluid upward at one side of the cell and cold fluid downward at the opposite side, one can detect the azimuthal orientation of the LSC by fitting

$$T_f = T_{w,k} + \delta_k \cos(i\pi/4 - \theta_{k,0}) \tag{2.1}$$

to all eight thermistors at one specific height and time. The integer i stands for the azimuthal location of the thermistors and takes values $i = 0 \ldots 7$, with the location of $i = 0$ located at a point directly east of the sample centre and i increasing in the counterclockwise direction when viewed from above. The index k denotes the vertical location of the thermistor and will in the following have letters b ($z = L/4$), m ($z = L/2$) and t ($z = 3L/4$). The orientation of the up-flow is given by the term $\theta_{k,0}$.

From the eight temperatures at a given k we computed the coefficients of the lowest four Fourier modes (Stevens, Clercx & Lohse 2011; Weiss & Ahlers 2011). This yielded all eight Fourier coefficients $A_{k,j}$ (the cosine coefficients) and $B_{k,j}$ (the sine coefficients), $j = 1, \ldots, 4$, and the corresponding 'energy' $E_{k,j}(t) = A_{k,j}^2 + B_{k,j}^2$. The time averages $\langle E_{k,j}(t) \rangle$ were summed to compute the total energy $E_{k,tot}$.

3. Results

3.1. *Orientation and energy of the large-scale circulation*

Probability distributions $p(\theta_{k,0}/2\pi)$ for the three levels $k = b, m, t$ are shown in figure 1 for (*a*) the classical and (*b*) the ultimate state. One sees a coherent orientation over the height of the sample. We fitted the function

$$p_f(\theta_k) = p_{k,0} \exp[(\theta_k - \theta_{k,0})^2/(2\sigma_k)^2] \tag{3.1}$$

to the data for $p(\theta_k)$. The results for $\theta_{k,0}$ and σ_k are shown in figure 2(*a*,*b*) as a function of Ra. Consistent with the predictions of Brown & Ahlers (2006*a*) for the influence of the Earth's Coriolis force, the orientation $\theta_{k,0}$ of the LSC up-flow is close to west (π) for all Ra. The width is slightly larger near the top and bottom

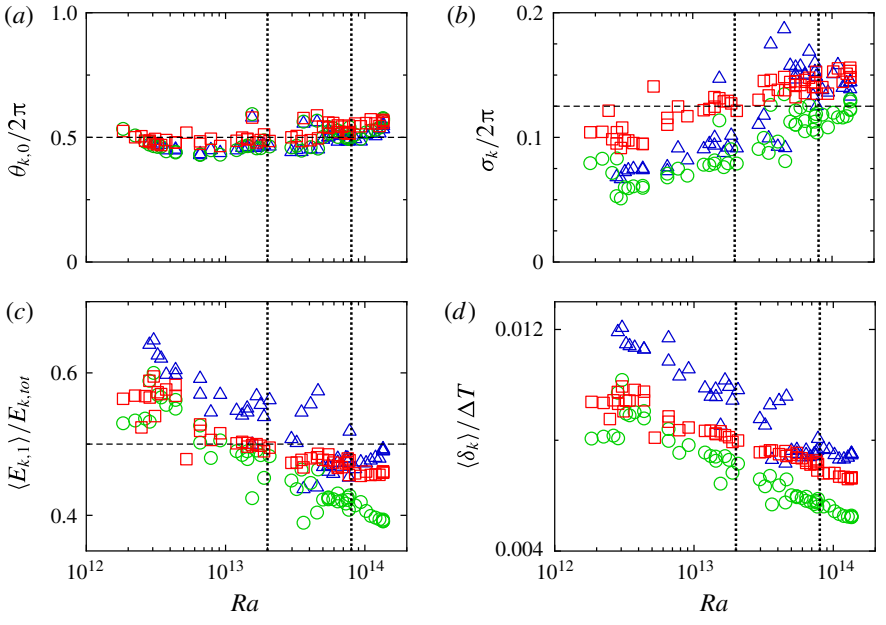

FIGURE 2. (*a*) Preferred orientation $\theta_{k,0}/(2\pi)$, (*b*) width $\sigma_k/(2\pi)$ of $p(\theta_k/2\pi)$, (*c*) LSC fundamental-mode energy $\langle E_{k,1}\rangle/E_{k,tot}$ and (*d*) LSC temperature amplitude $\langle\delta_k\rangle/\Delta T$ as a function of Ra for $z/L = 0.25$ (red squares), 0.50 (green circles) and 0.75 (blue triangles). The vertical dotted lines indicate $Ra_1^* = 2\times10^{13}$ and $Ra_2^* = 8\times10^{13}$ from figure 4 below. The horizontal dashed line in (*a*) indicates $\theta_{k,0} = \pi$ (west).

of the sample than it is in the middle, but the variation is not large. The relative contribution $\langle E_{k,1}\rangle = \langle\delta_k^2\rangle$ to the total fluctuation energy in a horizontal plane and near the sidewall (figure 2*c*) and the temperature amplitude $\langle\delta_k\rangle/\Delta T$ (figure 2*d*) are also nearly independent of z. Although $\langle E_{1,k}\rangle/E_{tot,k} \simeq 0.5$ and $\langle\delta_k\rangle/\Delta T \simeq 0.01$ are smaller than they are for smaller Ra and larger Pr (see, e.g., Brown & Ahlers (2007*b*) and Weiss & Ahlers (2011) and references therein), the coherence of all measured quantities over all three levels indicates the existence of a statistically well-defined, albeit highly fluctuating, single-roll LSC. All parameters depend only mildly upon Ra. There is no strong signature of the ultimate-state transition, but the larger scatter for $Ra_1^* \lesssim Ra \lesssim Ra_2^*$ and the much smaller scatter for $Ra > Ra_2^*$ are remarkable.

3.2. *The azimuthal diffusivity of the large-scale-circulation plane*

For a diffusive process in a system with a flat (constant) potential the root-mean-square (r.m.s.) azimuthal displacement

$$\Delta\theta_k \equiv \sqrt{\langle[\theta_{k,0}(t+n\delta t) - \theta_{k,0}(t)]^2\rangle}\ , \tag{3.2}$$

computed over various time intervals $n\delta t$, is given by

$$\Delta\theta_k = \sqrt{D_{\theta_k}(n\delta t)}. \tag{3.3}$$

Here, D_{θ_k} is the azimuthal diffusivity, δt is the time interval between successive data points, n is a positive integer and $\langle\,\rangle$ indicates a time average.

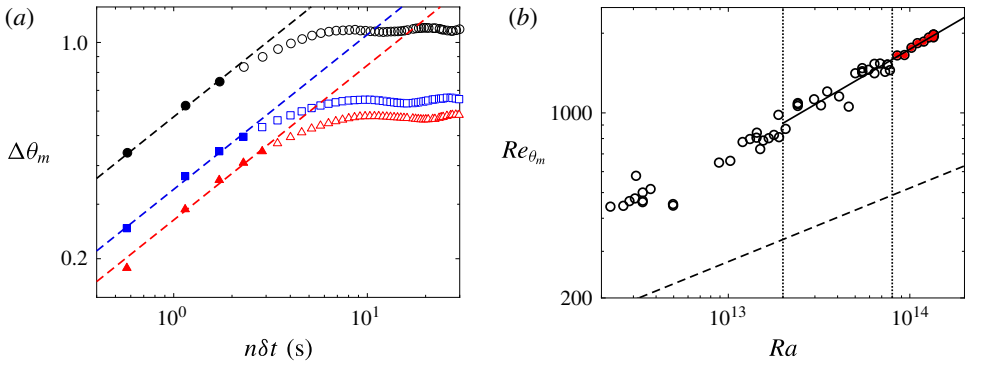

FIGURE 3. (*a*) The r.m.s. azimuthal displacement $\Delta\theta_m$ at $z/L = 0.50$ as a function of $n\delta t$ on logarithmic scales for $z/L = 0.5$ and $Ra = 1.35 \times 10^{14}$ (black circles), 1.90×10^{13} (blue squares) and 2.24×10^{12} (red triangles). The dashed lines are fits of the function $\Delta\theta_m = \sqrt{D_{\theta_m}(n\delta t)}$ to the solid symbols, adjusting only D_{θ_m}. (*b*) The Reynolds number $Re_{\theta_m} \equiv L\sqrt{D_{\theta_m}/\nu}$ as a function of Ra for $z/L = 0.50$. The solid line is a power-law fit (which gave an exponent of 0.40) to the circles with red dots. The dashed line indicates $Re_{\theta_m} = 0.0211 Ra^{0.278}$ from Brown & Ahlers (2006*b*) for $Pr = 4.38$. The vertical dotted lines represent $Ra_1^* = 2 \times 10^{13}$ and $Ra_2^* = 8 \times 10^{13}$.

Results for $\Delta\theta_m$ as a function of $n\delta t$ for $z/L = 0.50$ are shown in figure 3(*a*) for three values of Ra. One sees that the square-root law holds for small $n\delta t$, but that at large time intervals $\Delta\theta$ becomes constant. This is because the azimuthal potential had a minimum rather than being flat, as can be inferred from the probability distributions $p(\theta_{m,0})$ shown in figure 1. In that case diffusion in the potential well was limited to a finite range approximately equal to σ_m (Brown & Ahlers 2006*a*) (see figure 2*b*). One can still obtain values of D_{θ_m} from a fit of (3.3) to data at small $n\delta t$ such as those shown as solid symbols in figure 3(*a*). The corresponding results for Re_{θ_m} are shown in figure 3(*b*).

The dashed line in figure 3(*b*) is an extrapolation of the results obtained by Brown & Ahlers (2006*b*) for $Ra \lesssim 10^{11}$ and $Pr = 4.38$. Although our data are at much larger Ra, we note that this extrapolation can be made to pass through our data for classical RBC ($Ra \lesssim 2 \times 10^{13}$) when $Re_{\theta_m} Pr^{1.2}$ is plotted versus Ra, as in figure 4(*a*). We note that the same dependence on $Pr^{1.2}$ was found also for the velocity-fluctuation Reynolds number Re_V in the range $Pr \lesssim 7$ (He *et al.* 2015).

3.3. *The Nu, Re_V and Re_θ, and the ultimate-state transition range from Ra_1^* to Ra_2^**

In figure 4(*a*) one sees that there is a change in the Ra dependence of $Re_{\theta_m} Pr^{1.2}$ near $Ra = 2 \times 10^{13}$ which we identify with the beginning of the transition range to the ultimate state of RBC at Ra_1^* (left vertical dotted line). This becomes more obvious when the reduced data for $Re_{\theta_m} Pr^{1.2}/Ra^{0.4}$ are plotted, as in figure 4(*b*). There one also sees that the scatter in the data suddenly decreases as Ra exceeds $Ra_2^* \simeq 8 \times 10^{13}$, as was the case for Re_V (see, e.g., He *et al.* 2012*b*), and for $\langle E_{k,1}\rangle/E_{k,tot}$ in figure 2(*c*) shown above. The origin of the scatter in the transition region is unclear. One reason could be that between the classical and ultimate states the system can choose from two or more states with different BL configurations where the BLs are, spatially, neither entirely laminar nor entirely turbulent. Above the transition the fluctuations in the data

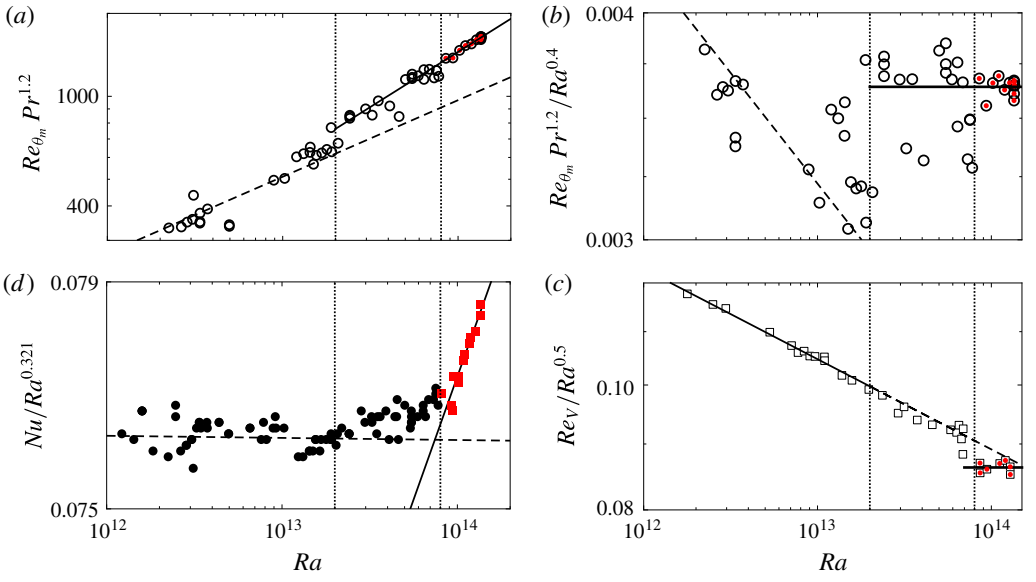

FIGURE 4. (*a*) A plot of $Re_{\theta_m} Pr^{1.2}$ as a function of Ra for $z/L = 0.50$ and $Pr \simeq 0.8$. The solid line is a power-law fit with an exponent of 0.40 to the circles with red dots. The dashed line represents $0.124 Ra^{0.278}$ as determined using the data from Brown & Ahlers (2006*b*) for $Pr = 4.38$. (*b*) The reduced Reynolds number $Re_{\theta_m} Pr^{1.2}/Ra^{0.4}$ as a function of Ra for $Pr \simeq 0.8$. The dashed line is an extrapolation of the results for $Pr = 4.38$ of Brown & Ahlers (2006*b*). The horizontal solid bar corresponds to 0.00364. (*c*) The reduced velocity-fluctuation Reynolds number $Re_V/Ra^{0.5}$ as a function of Ra from He *et al.* (2015). The solid line is the power-law fit to the data with $Ra \leqslant Ra_1^* = 2 \times 10^{13}$, which gave an exponent of 0.43. The dashed line is the extrapolation of that fit beyond Ra_1^*. The horizontal solid bar corresponds to 0.0863. (*d*) The reduced Nusselt number $Nu/Ra^{0.321}$ as a function of Ra on logarithmic scales. The solid line is the power-law fit $Nu = 0.0159 Ra^{0.370}$ to the red squares, and the horizontal dashed line is at $Nu/Ra^{0.321} = 0.0763$. In all panels the vertical dotted lines represent $Ra_1^* \simeq 2 \times 10^{13}$ and $Ra_2^* \simeq 8 \times 10^{13}$.

are small and the state seems to be uniquely defined. Further experiments are needed to better understand the transition region.

For larger Ra we find $Re_{\theta_m} Pr^{1.2} \propto Ra^{0.40 \pm 0.03}$, as shown by the solid black lines in figure 4(*a*,*b*). A theoretical explanation of the Ra and Pr dependence of Re_θ, in both the classical and the ultimate state, remains a challenge.

In figure 4(*c*) we show $Re_V/Ra^{0.50}$ from He *et al.* (2015). These data were taken in a different cell ('HPCF-IV'). While they did not give an obvious indication of Ra_1^* (except for a slight increase of the scatter), they clearly show a discontinuity and a change of the Ra dependence at $Ra_2^* \simeq 8 \times 10^{13}$. The Ra dependence $Re_V \propto Ra^{0.50 \pm 0.02}$ is in excellent agreement with the prediction by Grossmann & Lohse (2011) for the mean-flow Reynolds number Re_U in the ultimate state.

Figure 4(*d*) shows new Nu measurements for the same sample as used here ('HPCF-IVb') for the diffusivity measurements. One sees that $Nu/Ra^{0.321}$ is constant in the classical state, and begins to gently increase for $Ra > Ra_1^*$. For $Ra > Ra_2^*$ (red squares) we find $Nu \propto Ra^{0.37 \pm 0.02}$, also consistent with the prediction for the ultimate state (Grossmann & Lohse 2011).

The data in figure 4 clearly identify a transition to a new state of the system, with a transition range starting at $Ra_1^* \simeq 2 \times 10^{13}$. It is important to decide whether this Ra value is consistent with the BL shear instability associated with the ultimate-state transition. Since both the LSC and fluctuations are expected to contribute to the BL instability, we use the measured $Re_{eff} \equiv \sqrt{Re_U^2 + Re_V^2} = 1.00 \times Ra^{0.436}$ (He *et al.* 2015) for $\Gamma = 1.00$, which, for $Ra_1^* \simeq 2 \times 10^{13}$, gives $Re_{eff} = 6.3 \times 10^5$ and thus yields the shear Reynolds number (Grossmann & Lohse 2002) $Re_s^* \simeq 0.48\sqrt{Re_{eff}} \simeq 380$. While it is difficult to estimate the overall uncertainty of this value, it is generally consistent with the expected $Re_s^* \simeq 400$ (Landau & Lifshitz 1987).

4. Non-Oberbeck–Boussinesq effects and the Skrbek–Urban claim

Real systems will deviate from the OB approximation. Consequently, T_c may differ from T_m and various global and local properties may be affected. While in most experiments these effects are small and often negligible, Skrbek & Urban (2015) (SU) claimed that they have a large influence on the Göttingen Nu measurements, and that the observation of the ultimate-state transition based on those measurements may be illusory and a misinterpretation of non-OB effects (they make similar claims regarding the Grenoble measurements). In this section we shall show that the arguments of SU are flawed and that there is indeed no evidence that non-OB effects alter the original conclusions regarding the ultimate-state transition as discussed in part in § 3.3.

To lowest order, non-OB effects have no influence on Nu when the fluid properties are evaluated at T_m (Ahlers *et al.* 2006). The physics of this is simple. In the classical state one may, to a good approximation, regard Nu as proportional to the inverse of the sum of two resistors in series and carrying the same heat current. One (R_b) corresponds to the bottom and the other (R_t) to the top BL, and the turbulent bulk between the BLs is taken to be a perfect conductor. While one resistance (that of the thicker BL) is increased slightly by the non-OB conditions, the other is decreased slightly by a nearly equal amount, and their sum, and thus Nu, remains nearly the same. This is shown theoretically in § 4 of Ahlers *et al.* (2006). It is not only a theoretical result, but was also demonstrated experimentally by the same authors. Although one might think that this argument does not apply to the ultimate state where the turbulent BLs extend deep into the interior (Grossmann & Lohse 2011, 2012), in practice also there one finds most of the temperature drop across thin layers near the plates (Ahlers *et al.* 2012*a*), and the 'two-resistor model' remains reasonable at least for Ra not too much larger than Ra_2^*.

For the determination of Nu from the Göttingen measurements (Ahlers *et al.* 2012*b*; He *et al.* 2012*a*,*b*, 2015), which revealed the transition to the ultimate state, careful experimental consideration had been given to the need to correct for non-OB effects. Possible differences due to the definition of Ra were quite small since T_c was very close to T_m (He *et al.* (2012*a*) figure 1(*b*); see also He *et al.* (2013)), with $(T_c - T_m)/T_m \lesssim 0.002$ (temperatures are in Kelvin). With such a small change of the absolute temperature the properties of a gas do not vary significantly, and it does not matter, for instance, whether Ra is evaluated using the properties at T_m, as is customary and preferred theoretically, or at T_c, as suggested by SU. Further, it had been shown experimentally that non-OB effects did not influence the measurements significantly by comparing data at the same Ra taken with relatively large ΔT where non-OB effects are larger (by using relatively low pressures) with others taken with smaller ΔT where non-OB effects are smaller (measured at larger pressures) (figure B.1*b* of Ahlers *et al.* (2012*b*)).

Contrary to the above, SU claim that non-OB effects have a large influence on the Göttingen *Nu* data. They state that

> the claims of observing transition to the ultimate state of Rayleigh–Bénard convection could indeed be related to non-Oberbeck–Boussinesq effects.

They then propose a different method of analysis (the 'SU model'), which, they argue, corrects for these large non-OB effects. Below we show that the arguments of SU have two flaws.

The first flaw is that they arbitrarily decided that it would be better to evaluate the fluid properties at T_c (either experimentally measured or derived from a crude model) rather than at T_m. It has been known since the trailblazing work of Busse (1967) (see also Ahlers *et al.* 2009*a*) for convection near onset, which was extended to the turbulent state by Ahlers *et al.* (2006), that this is inappropriate. A more systematic approach is to retain T_m as the only *a priori* known reference temperature, and to treat non-OB effects with this choice as perturbations of the OB state. This systematic procedure will then yield a value of $T_c - T_m$ *a posteriori*. However, as indicated above and shown also by He *et al.* (2013), choosing T_c instead has in practice virtually no consequences for the Göttingen *Nu* and *Ra* values because $|(T_c - T_m)|/T_m$ was small. Nonetheless, there is no foundation for SU's choice of T_c rather than T_m, and it goes contrary to a large body of well-established literature.

The second flaw has a greater impact on the *Nu* and *Ra* values. Skrbek and Urban claim that in the Göttingen experiments

> T_t values are dangerously close to the SVP line (representing the equilibrium first-order liquid–gas phase transition where due to fluctuations condensation/evaporation could take place).

Let us restate the nature of first-order phase transitions. There is no anomalous increase of fluctuation intensities, and all properties vary only slowly with temperature until the very point where the transition temperature is crossed and latent-heat contributions to *Nu* occur. Thus, the claim by SU is unfounded. Skrbek and Urban then move on to claim

> We can further strengthen our argument by pointing out the work of Zhong, Funfschilling & Ahlers (2009), showing that the heat transfer efficiency would be considerably enhanced if condensation/evaporation processes were to take place in the vicinity of the SVP line at the top plate of the SF6 cell.

This is a misinterpretation of the cited paper. Zhong *et al.* (2009) showed that, with decreasing mean temperature, there is no excess contribution to the heat transport until the very point at which the top temperature T_t crosses the vapour-pressure curve at $T_\phi(P)$. When T_ϕ is crossed by T_t (which never happened in the Göttingen measurements), a continuous but sharp transition takes place to a state where the heat transport increases linearly with $T_\phi - T_t$.

Skrbek and Urban then continue to state

> Upon increasing *Ra*, the top half of the cell becomes affected by the non-Oberbeck–Boussinesq effects, while the bottom half, if lying sufficiently far away from the SVP curve, does not.

Needless to say, this is incorrect. All physical systems are influenced by non-OB effects; the question is only whether these effects influence a given measured quantity significantly. While the non-OB effect is indeed stronger at the top of the cell, it does not vanish in the bottom, and for the Göttingen data (by any reasonable measure) is smaller by less than a factor of two or so.

Skrbek and Urban then argue that

> one can avoid the non-Oberbeck–Boussinesq effects in the top half of the cell, by replacing it with the inverted (with respect to T_c) nearly Oberbeck–Boussinesq bottom half.

This argument is at odds with the beautiful cancellation between the increase of R_b and decrease of R_t characteristic of non-OB systems as discussed above, and creates a qualitatively new fictitious system in which Nu is proportional to $1/(2R_b)$ rather than to $1/(R_b + R_t)$ as is the case in the physical system! To make things worse, they then replace $\Delta T \equiv T_b - T_t$ by $\Delta T_{eff} = 2(T_b - T_c)$. This SU model yields values of Nu and Ra that are unrelated to reality.

It is amusing (but unrelated to the present discussion) that a non-OB system with BLs that have properties that are reflection symmetric about the horizontal mid plane of the sample does indeed exist. It occurs above the critical pressure of a fluid when, at constant pressure, the top and bottom temperatures are on opposite sides of and approximately equidistant from the temperature on the critical isochore (Ahlers *et al.* 2008, 2009*a*; Burnishev, Segre & Steinberg 2010; Burnishev & Steinberg 2012).

Beyond their claims for the influence of non-OB effects on Nu, SU also state that

> It is important to emphasize that not only the Nusselt number scaling, but the scaling of any other independently measured quantity, such as the Reynolds number $Re = Re(Ra)$, that might have displayed 'phase transitions' spuriously interpreted as independent confirmation of the transition to the ultimate regime, will change, as well.

We do not agree with this statement. The Nu is determined largely by the boundary layers with their steep thermal gradients, while recent Re_V measurements (He *et al.* 2015), as well as the diffusivity measurements presented here, are properties of the bulk which depend only on the local temperature which is nearly uniform and close to T_c (and T_c in turn is nearly equal to T_m). In the SU model the major influence on $Re(Ra)$ arises from using ΔT_{eff} rather than ΔT to calculate Ra, and, as just stated, this use leads to an unphysical model for RBC.

From the above discussion one can see that the data manipulation of SU leads to a fictitious system which is unrelated to those investigated in Grenoble and Göttingen. Thus, we see no validity in questioning the claim, based on the Göttingen data, that a transition to a new state of RBC has been observed and that this state has been at least partially characterized.

5. Summary and conclusions

In this paper we presented new measurements of the temperature amplitude and of the azimuthal diffusivity of the large-scale circulation for a cylindrical sample with $\Gamma = 1.00$ which show the ultimate-state transition range from $Ra_1^* \simeq 2 \times 10^{13}$ to $Ra_2^* \simeq 8 \times 10^{13}$, in agreement with findings based on measurements of Nu and of the velocity-fluctuation Reynolds number Re_V.

We also showed that the claim by Skrbek & Urban (2015) that 'observing transition to the ultimate state could indeed be related to non-Oberbeck–Boussinesq effects' is without any foundation.

Finally, we note that turbulent circular Couette flow (CCF) was shown to have equations of motion equivalent to those of turbulent RBC (Eckhardt, Grossmann & Lohse 2007). Experiments for this system yielded a 'Nusselt number' $Nu_\omega \propto Ta^{0.38}$ which characterizes the angular velocity transport (van Gils *et al.* 2011). Here, the Taylor number Ta plays a role equivalent to Ra in RBC. A so-called 'wind Reynolds number', analogous to the Reynolds number in RBC, was found to be proportional to $Ta^{0.50}$ (Huisman *et al.* 2012). Both of these results agree with the analogous ultimate-state results for RBC shown in figure 4(*c*,*d*). Thus, there is strong evidence that both RBC and CCF, at high enough driving, enter equivalent states which have properties expected of an ultimate state with turbulent boundary layers (Grossmann & Lohse 2011). Further, it is worth noting that for both systems the ultimate state is entered at approximately the same value, close to 400, of the boundary-layer shear Reynolds number (for RBC see § 3.3 in the present paper and He *et al.* (2012*b*); for CCF see § 5 and figure 14(*b*) of Ostilla *et al.* (2013), as well as van Gils *et al.* (2012), Ostilla-Monico *et al.* (2014) and Grossmann, Lohse & Sun (2016)), where the transition to a turbulent BL is expected (Landau & Lifshitz 1987).

Acknowledgements

We are grateful to the Max Planck Society and the Volkswagen Stiftung, whose support made the establishment of the Uboot facility and the experiments possible. We thank the Deutsche Forschungsgemeinschaft (DFG) for financial support through SFB963: 'Astrophysical Flow Instabilities and Turbulence'. X.H. acknowledges support through the Chinese Thousand Young Talents Program. The work of G.A. was supported in part by the US National Science Foundation through grant DMR11-58514.

References

Ahlers, G. 2009 Turbulent convection. *Physics* **2**, 74.

Ahlers, G., Bodenschatz, E., Funfschilling, D., Grossmann, S., He, X., Lohse, D., Stevens, R. & Verzicco, R. 2012*a* Logarithmic temperature profiles in turbulent Rayleigh–Bénard convection. *Phys. Rev. Lett.* **109**, 114501.

Ahlers, G., Bodenschatz, E. & He, X. 2014 Logarithmic temperature profiles of turbulent Rayleigh–Bénard convection in the classical and ultimate state for a Prandtl number of 0.8. *J. Fluid Mech.* **758**, 436–467.

Ahlers, G., Brown, E., Fontenele Araujo, F., Funfschilling, D., Grossmann, S. & Lohse, D. 2006 Non-Oberbeck–Boussinesq effects in strongly turbulent Rayleigh–Bénard convection. *J. Fluid Mech.* **569**, 409–445.

Ahlers, G., Calzavarini, E., Fontenele Araujo, F., Funfschilling, D., Grossmann, S., Lohse, D. & Sugiyama, K. 2008 Non-Oberbeck–Boussinesq effects in turbulent thermal convection in ethane close to the critical point. *Phys. Rev.* E **77**, 046302.

Ahlers, G., Dressel, B., Oh, J. & Pesch, W. 2009*a* Strong non-Boussinesq effects near the onset of convection in a fluid near its critical point. *J. Fluid Mech.* **642**, 15–48.

Ahlers, G., Funfschilling, D. & Bodenschatz, E. 2009*b* Transitions in heat transport by turbulent convection for $Pr = 0.8$ and $10^{11} \leqslant Ra \leqslant 10^{15}$. *New J. Phys.* **11**, 123001.

Ahlers, G., Grossmann, S. & Lohse, D. 2009*c* Heat transfer and large scale dynamics in turbulent Rayleigh–Bénard convection. *Rev. Mod. Phys.* **81**, 503–538.

AHLERS, G., HE, X., FUNFSCHILLING, D. & BODENSCHATZ, E. 2012*b* Heat transport by turbulent Rayleigh–Bénard convection for $Pr \simeq 0.8$ and $3 \times 10^{12} \lesssim Ra \lesssim 10^{15}$: aspect ratio $\gamma = 0.50$. *New J. Phys.* **14**, 103012.

BOUSSINESQ, J. 1903 *Theorie Analytique de la Chaleur*, vol. 2. Gauthier-Villars.

BROWN, E. & AHLERS, G. 2006*a* Effect of the Earth's Coriolis force on turbulent Rayleigh–Bénard convection in the laboratory. *Phys. Fluids* **18**, 125108.

BROWN, E. & AHLERS, G. 2006*b* Rotations and cessations of the large-scale circulation in turbulent Rayleigh–Bénard convection. *J. Fluid Mech.* **568**, 351–386.

BROWN, E. & AHLERS, G. 2007*a* Large-scale circulation model of turbulent Rayleigh–Bénard convection. *Phys. Rev. Lett.* **98**, 134501.

BROWN, E. & AHLERS, G. 2007*b* Temperature gradients, and search for non-Boussinesq effects, in the interior of turbulent Rayleigh–Bénard convection. *Europhys. Lett.* **80**, 14001.

BROWN, E. & AHLERS, G. 2008 A model of diffusion in a potential well for the dynamics of the large-scale circulation in turbulent Rayleigh–Bénard convection. *Phys. Fluids* **20**, 075101.

BROWN, E., NIKOLAENKO, A. & AHLERS, G. 2005 Reorientation of the large-scale circulation in turbulent Rayleigh–Bénard convection. *Phys. Rev. Lett.* **95**, 084503.

BURNISHEV, Y., SEGRE, E. & STEINBERG, V. 2010 Strong symmetrical non-Oberbeck–Boussinesq turbulent convection and the role of compressibility. *Phys. Fluids* **22**, 035108.

BURNISHEV, Y. & STEINBERG, V. 2012 Statistics and scaling properties of temperature field in symmetrical non-Oberbeck–Boussinesq turbulent convection. *Phys. Fluids* **24**, 045102.

BUSSE, F. H. 1967 The stability of finite amplitude cellular convection and its relation to an extremum principle. *J. Fluid Mech.* **30**, 625–649.

CHAVANNE, X., CHILLA, F., CASTAING, B., HEBRAL, B., CHABAUD, B. & CHAUSSY, J. 1997 Observation of the ultimate regime in Rayleigh–Bénard convection. *Phys. Rev. Lett.* **79**, 3648–3651.

CHAVANNE, X., CHILLA, F., CHABAUD, B., CASTAING, B. & HEBRAL, B. 2001 Turbulent Rayleigh–Bénard convection in gaseous and liquid He. *Phys. Fluids* **13**, 1300–1320.

CHILLÀ, F. & SCHUMACHER, J. 2012 New perspectives in turbulent Rayleigh–Bénard convection. *Eur. Phys. J.* E **35**, 58.

ECKHARDT, B., GROSSMANN, S. & LOHSE, D. 2007 Torque scaling in turbulent Taylor–Couette flow between independently rotating cylinders. *J. Fluid Mech.* **581**, 221–250.

VAN GILS, D. P. M., HUISMAN, S. G., BRIGGERT, G.-W., SUN, C. & LOHSE, D. 2011 Torque scaling in turbulent Taylor–Couette flow with co- and counterrotating cylinders. *Phys. Rev. Lett.* **106**, 024502.

VAN GILS, D., HUISMAN, S., GROSSMANN, S., SUN, C. & LOHSE, D. 2012 Optimal Taylor–Couette turbulence. *J. Fluid Mech.* **706**, 118–149.

GROSSMANN, S. & LOHSE, D. 2002 Prandtl and Rayleigh number dependence of the Reynolds number in turbulent thermal convection. *Phys. Rev.* E **66**, 016305.

GROSSMANN, S. & LOHSE, D. 2011 Multiple scaling in the ultimate regime of thermal convection. *Phys. Fluids* **23**, 045108.

GROSSMANN, S. & LOHSE, D. 2012 Logarithmic temperature profiles in the ultimate regime of thermal convection. *Phys. Fluids* **24**, 125103.

GROSSMANN, S., LOHSE, D. & SUN, C. 2016 High Reynolds number Taylor–Couette turbulence. *Annu. Rev. Fluid Mech.* **48**, 53–80.

HE, X., FUNFSCHILLING, D., BODENSCHATZ, E. & AHLERS, G. 2012*a* Heat transport by turbulent Rayleigh–Bénard convection for $Pr \simeq 0.8$ and $4 \times 10^{11} \lesssim Ra \lesssim 2 \times 10^{14}$: ultimate-state transition for aspect ratio $\gamma = 1.00$. *New J. Phys.* **14**, 063030.

HE, X., FUNFSCHILLING, D., NOBACH, H., BODENSCHATZ, E. & AHLERS, G. 2012*b* Transition to the ultimate state of turbulent Rayleigh–Bénard convection. *Phys. Rev. Lett.* **108**, 024502.

HE, X., FUNFSCHILLING, D., NOBACH, H., BODENSCHATZ, E. & AHLERS, G. 2013 Comment on 'Effect of boundary layers asymmetry on heat transfer efficiency in turbulent Rayleigh–Bénard convection at very high Rayleigh numbers by Urban *et al.*?'. *Phys. Rev. Lett.* **110**, 199401.

HE, X., VAN GILS, D., BODENSCHATZ, E. & AHLERS, G. 2014 Logarithmic spatial variations and universal f^{-1} power spectra of temperature fluctuations in turbulent Rayleigh–Bénard convection. *Phys. Rev. Lett.* **112**, 174501.

HE, X., VAN GILS, D., BODENSCHATZ, E. & AHLERS, G. 2015 Reynolds numbers and the elliptic approximation near the ultimate state of turbulent Rayleigh–Bénard convection. *New J. Phys.* **17**, 063028.

HUISMAN, S. G., VAN GILS, D. P. M., GROSSMANN, S., SUN, C. & LOHSE, D. 2012 Ultimate turbulent Taylor–Couette flow. *Phys. Rev. Lett.* **108**, 024501.

KADANOFF, L. P. 2001 Turbulent heat flow: structures and scaling. *Phys. Today* **54** (8), 34–39.

KRAICHNAN, R. H. 1962 Turbulent thermal convection at arbitrary Prandtl number. *Phys. Fluids* **5**, 1374–1389.

LANDAU, L. D. & LIFSHITZ, E. M. 1987 *Fluid Mechanics*. Pergamon.

LOHSE, D. & XIA, K.-Q. 2010 Small-scale properties of turbulent Rayleigh–Bénard convection. *Annu. Rev. Fluid Mech.* **42**, 335–364.

OBERBECK, A. 1879 Über die Wärmeleitung der Flüssigkeiten bei Berücksichtigung der Strömungen infolge von Temperaturdifferenzen. *Ann. Phys. Chem.* **7**, 271–292.

OSTILLA, R., STEVENS, R., GROSSMANN, S., VERZICCO, R. & LOHSE, D. 2013 Optimal Taylor–Couette flow: direct numerical simulation. *J. Fluid Mech.* **719**, 14–46.

OSTILLA-MONICO, R., VAN DER POEL, E., VERZICCO, R., GROSSMANN, S. & LOHSE, D. 2014 Exploring the phase diagram of fully turbulent Taylor–Couette flow. *J. Fluid Mech.* **761**, 1–26.

ROCHE, P.-E., GAUTHIER, F., KAISER, R. & SALORT, J. 2010 On the triggering of the ultimate regime of convection. *New J. Phys.* **12**, 085014.

SKRBEK, L. & URBAN, P. 2015 Has the ultimate state of turbulent thermal convection been observed? *J. Fluid Mech.* **785**, 270–282.

SPIEGEL, E. A. 1971 Convection in stars. *Annu. Rev. Astron. Astrophys.* **9**, 323–352.

STEVENS, R. J., CLERCX, H. J. & LOHSE, D. 2011 Effect of plumes on measuring the large scale circulation. *Phys. Fluids* **23**, 095110.

WEI, P. & AHLERS, G. 2014 Logarithmic temperature distribution in the bulk of turbulent Rayleigh–Bénard convection for a Prandtl number of 12.3. *J. Fluid Mech.* **758**, 809–830.

WEISS, S. & AHLERS, G. 2011 The large-scale flow structure in turbulent rotating Rayleigh–Bénard convection. *J. Fluid Mech.* **688**, 461–492.

ZHONG, J.-Q., FUNFSCHILLING, D. & AHLERS, G. 2009 Enhanced heat transport by turbulent two-phase Rayleigh–Bénard convection. *Phys. Rev. Lett.* **102**, 124501.